Volume 5 · No. 23 – December 4 2009

D15063

NANO small MICRO

www.small-journal.com

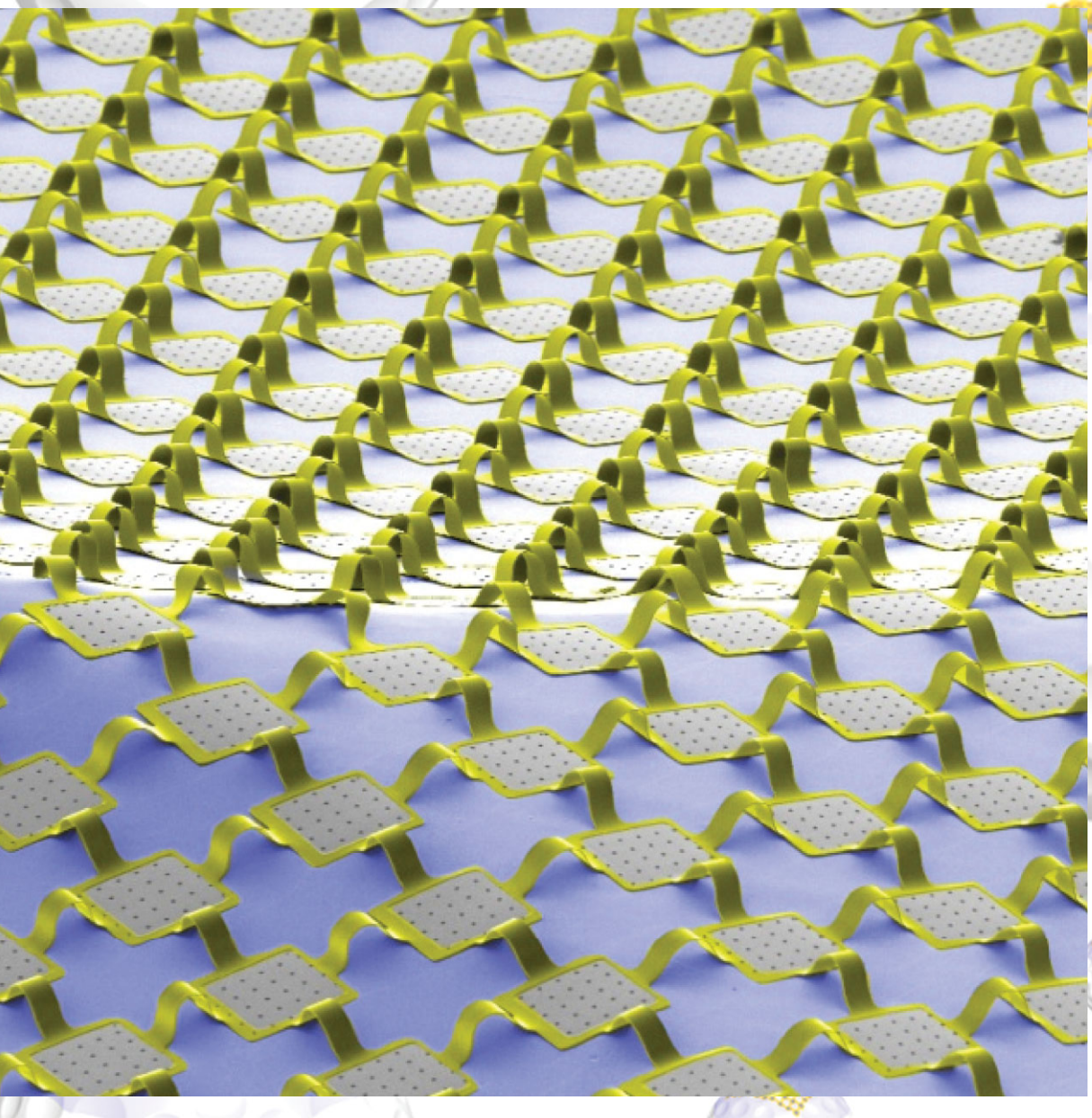

23/2009

WILEY-VCH

Curvilinear Electronics Formed Using Silicon Membrane Circuits and Elastomeric Transfer Elements

S. Ha, Y. Huang, J. A. Rogers, et al.

small NANO MICRO

Curvilinear Electronics Formed Using Silicon Membrane Circuits and Elastomeric Transfer Elements

Heung Cho Ko, Gunchul Shin, Shuodao Wang, Mark P. Stoykovich, Jeong Won Lee, Dong-Hun Kim, Jeong Sook Ha, Yonggang Huang,* Keh-Chih Hwang, and John A. Rogers**

***M**aterials and methods to achieve electronics intimately integrated on the surfaces of substrates with complex, curvilinear shapes are described. The approach exploits silicon membranes in circuit mesh structures that can be deformed in controlled ways using thin, elastomeric films. Experimental and theoretical studies of the micromechanics of such curvilinear electronics demonstrate the underlying concepts. Electrical measurements illustrate the high yields that can be obtained. The results represent significant experimental and theoretical advances over recently reported concepts for creating hemispherical photodetectors in electronic eye cameras and for using printable silicon nanoribbons/membranes in flexible electronics. The results might provide practical routes to the integration of high performance electronics with biological tissues and other systems of interest for new applications.*

Keywords:
- conformal wrapping
- curvilinear electronics
- elastomeric transfer
- micromechanics
- silicon membranes

1. Introduction

All dominant forms of electronics and optoelectronics exist exclusively in planar layouts on the flat surfaces of rigid, brittle semiconductor wafers or glass plates. Although these 2D configurations are well-suited for many existing applications, they are intrinsically incompatible with many envisioned systems of the future. For example, they do not enable natural integration with the soft, curvilinear surfaces of living organisms (e.g., body parts) for the purposes of health monitoring or therapeutics. They also preclude the use of many interesting, often biologically inspired, non-planar device

[*] Prof. J. A. Rogers, Dr. H. C. Ko[+], M. P. Stoykovich[‡]
Department of Materials Science and Engineering
Frederick Seitz Materials Research Laboratory
Beckman Institute for Advanced Science and Technology
University of Illinois at Urbana-Champaign
Urbana, IL 61801 (USA)
E-mail: jrogers@uiuc.edu

Prof. J. S. Ha, G. Shin
Department of Chemical and Biological Engineering
Korea University
Seoul 136-701 (Korea)
E-mail: jeongsha@korea.ac.kr

Prof. Y. Huang, S. Wang
Department of Mechanical Engineering
Department of Civil and Environmental Engineering
Northwestern University
Evanston, IL 60208 (USA)
E-mail: y-huang@northwestern.edu

J. W. Lee, D.-H.Kim
Department of Materials Science and Engineering
Pohang University of Science and Technology (POSTECH)
Pohang, Gyungbuk 790-784 (Korea)

Prof. K.-C. Hwang
Department of Engineering Mechanics
Tsinghua University
Beijing 100084 (China)

[+] Present Address: Department of Materials Science and Engineering
Gwangju Institute of Science and Technology (GIST)
Gwangju 500-712 (Korea)

[‡] Present Address: Department of Chemical and Biological Engineering
University of Colorado – Boulder Boulder, Colorado 80309 (USA)

Supporting Information is available on the WWW under http://www.small-journal.com or from the author.

DOI: 10.1002/smll.200900934

designs such as those based on curved focal plane arrays[1–6] as recently demonstrated in fully functional hemispherical electronic eye cameras.[6] Such curvilinear systems cannot be achieved easily using existing technologies due to the inherently 2D nature of established device processing procedures, ranging from deposition, growth, etching, and doping to photolithography. Approaches that use unusual electronic materials[3,4,7] or patterning techniques[3,4,5,8] might be useful, but they require substantial further development for high performance applications.

We present in this paper advanced concepts for conformal wrapping of silicon-based circuits, initially fabricated in 2D layouts with standard or moderately adapted forms of conventional techniques, onto surfaces with a range of curvilinear shapes. The strategy uses structured silicon membranes with thin polymer/metal interconnects, in non-coplanar mesh layouts. The result embodies combined aspects of concepts recently reported for electronic eye cameras and for stretchable electronics to achieve new and general capabilities for curvilinear electronics on surfaces with nearly arbitrary shapes. Supporting theoretical mechanics models provide insights into the basic phenomena, as well as subtle aspects. Quantitative agreement between predictions of these models and measured characteristics of wrapped systems on diverse classes of substrates validates the approaches and also establishes engineering design rules for future work.

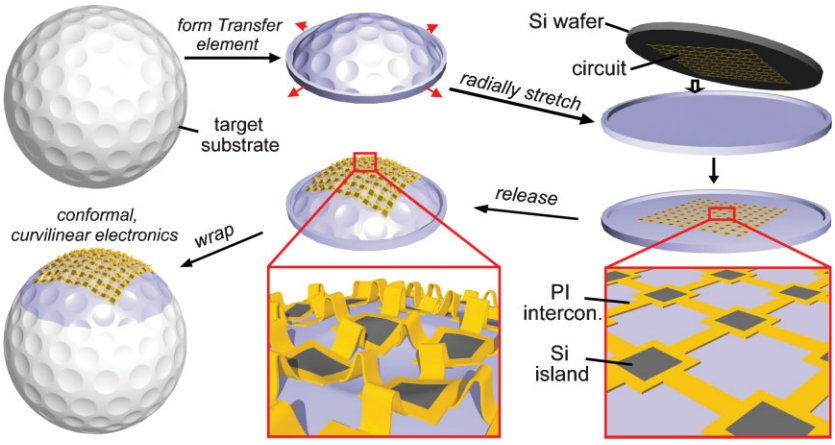

Figure 1. Schematic illustration of steps for using silicon membrane circuits in mesh layouts (i.e., arrays of islands interconnected by narrow strips) and elastomeric transfer elements to wrap electronics onto substrates with complex, curvilinear shapes, such as the dimpled surface of the golf ball shown here (upper left). The process begins with fabrication of a thin transfer element in an elastomer such as PDMS by double-casting and thermal-curing against the object to be wrapped (i.e., the target substrate) (top middle). Radially stretching the resulting element from its rim forms a flat drumhead membrane in which all points in the PDMS are in tension with levels of strain that vary with position. Contacting this stretched transfer element against a prefabricated circuit in a planar, ultrathin mesh geometry on a silicon wafer and then peeling it back lifts the circuit onto the PDMS (top right). Relaxing the tension geometrically transforms the membrane and the circuit on its surface into the shape of the target substrate (bottom middle). During this process, the interconnection bridges of the mesh adopt non-coplanar arc shapes (bottom middle inset), thereby accommodating the compressive forces in a way that avoids significant strains in the islands. Transfer to the corresponding region of the target substrate and removal of the rim completes the process (bottom left).

2. Results and Discussion

Figure 1 provides a schematic illustration of the process for the case of conformal integration of circuits on the surface of a golf ball, which we will generically refer to as the target substrate. The approach, which represents a generalization of procedures that we reported recently,[6] begins with the formation of a thin, elastomeric membrane of poly(dimethylsiloxane) (PDMS) by double casting and thermal curing against the target substrate to replicate its surface geometry.

Mounting in a tensioning stage that applies radially directed force at the rim with ten coordinated paddle arms pulls the thin, structured PDMS membrane into the flat shape of a drumhead in a manner that places all points under net tensile strain. In the next step, this tensioned transfer element contacts a separately fabricated silicon membrane circuit mesh supported by, but not strongly adhered to, the surface of a silicon wafer (i.e., handle wafer of the silicon-on-insulator (SOI) substrate). Peeling the transfer element back from the wafer lifts the circuit onto the flat, soft surface of the PDMS membrane in a nondestructive manner via the action of van der Waals forces complemented in some cases by –Si–O–Si– interfacial bonds that form upon reaction between –OH groups on the PDMS and SiO_2 surfaces of the transfer element and the island regions of the circuit mesh, respectively. Releasing the tensioning stage causes the PDMS to relax elastically back to its original shape, carrying the circuit mesh along with it. During this process, the silicon islands move closer together with magnitudes that can correspond to significant compressive strains (several tens of percent, depending on the radial pre-extension). The thin polyimide (PI) interconnect lines accommodate this motion by delaminating from the PDMS to adopt non-coplanar arc shapes. This process accomplishes the geometrical transformation from flat to curvilinear layouts without inducing significant strains in the silicon regions of the circuit mesh. In the final step, the structure is aligned and adhered to the target substrate and the rim structure is cut away. Experimental demonstrations and theoretical analyses described in the following reveal essential details of this strategy.

Figure 2 summarizes an experimental example corresponding to the system of Figure 1 with a mesh that consists of a square array of square islands of silicon (100 μm by 100 μm; pitch 250 μm; thickness 700 nm) and PI interconnects (width: 30 μm; length: 150 μm; thickness 1.4 μm). Figure 2a and b shows optical images of the mesh on a transfer element in the geometry of a golf ball (Titanium, Winfield) and after integration with the ball. The dimples in this particular type of golf ball (diameter ≈ 4.3 cm) have diameters and depths of ≈3.6 and ≈0.26 mm, respectively, and they have approximately spherical curvature. Scanning electron microscopy (SEM) images reveal

NANO MICRO small

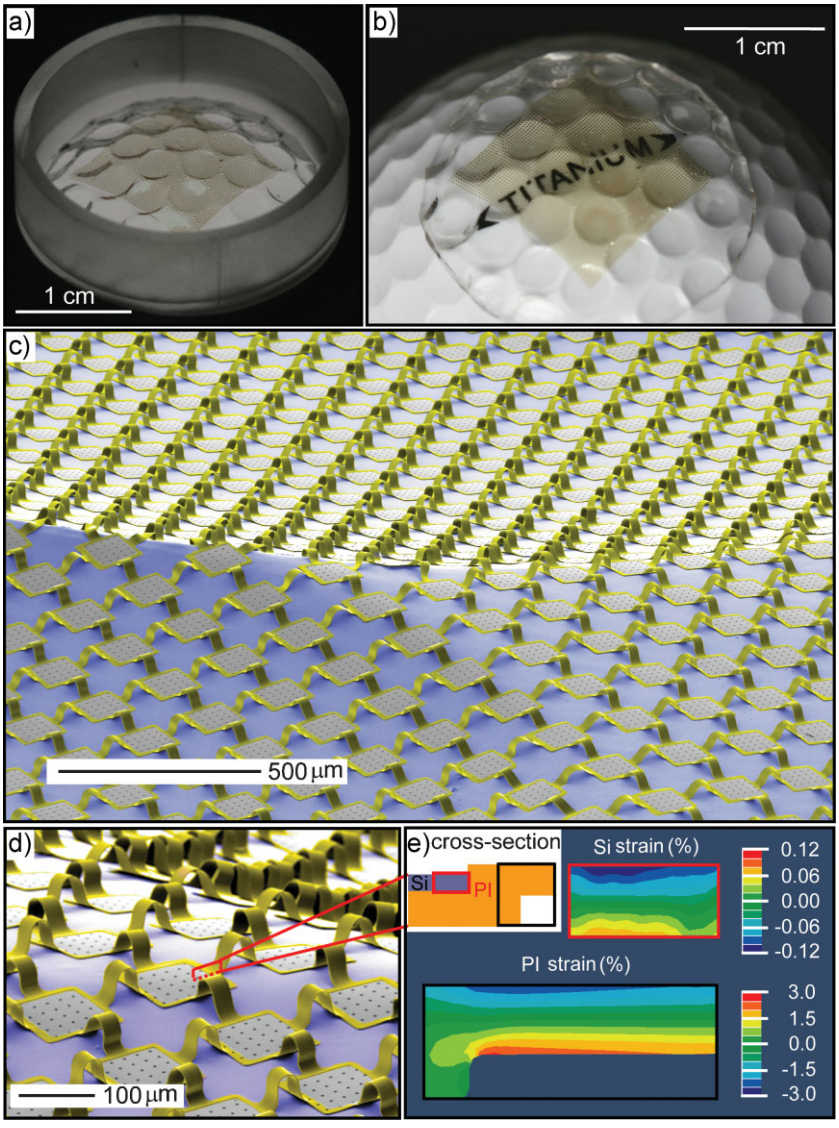

Figure 2. Photographs of a silicon circuit mesh on the surface of a PDMS transfer element with the surface shape of a golf ball before (a) and after (b) contacting this element to the corresponding region of the ball and cutting away the rim. c,d) Angled-view SEM images of the sample shown in (a). The images were colorized to enhance the contrast between the various regions. The gray, yellow, and blue colors correspond to silicon, PI, and PDMS, respectively. e) Strain distribution obtained by the finite element method in the silicon and PI regions at the cross-sectional area highlighted in (d).

that compression of the mesh associated with the geometry transformation can, according to the magnitude of the applied tension, range from ≈20% to ≈60%, depending on position across the structure. The overall coverage of the silicon in the curvilinear layout corresponds to ≈26% of the total area. The images indicate remarkably high levels of uniformity in the wrapped circuit. In certain cases, we observed partial detachment of some fraction of the silicon islands located on the most highly curved areas, that is, the rim edges of the dimples (see Supporting Information). We did not, however, observe cracking or any other related mechanical failures in the silicon or the PI anywhere in these systems.

Full mechanics analysis provides important insights. We used, in particular, the finite element method to study the PDMS transfer element (Young's modulus 2.0 MPa; Poisson's ratio 0.48; center thickness 300 μm) as the rim is stretched from 23.1 to 29.2 mm for this golf ball case. Here, the strain in the PDMS reaches a maximum of 15.9% along the circumferential direction just inside the rim edges of the dimples, though the circumferential strain is fairly uniform at 13.2% ≈ 15.9%. The meridional strain varies from 15.5% at the center to a compressive strain −5.5% at the rim edges of the dimples. After transfer of the silicon circuit mesh, release of the membrane creates a maximum strain of 0.12% in the silicon membrane islands (Figure 2e), which is much below the fracture strain (1%). The maximum strain in the PI is 2.7% (Figure 2e), considerably below the fracture strain for this material (≈7%) (see Supporting Information).

Figure 3 shows an example of wrapping the same type of circuit mesh onto a conical substrate (diameter of base ≈23.6 mm; height ≈6.5 mm; radius of curvature at the tip ≈2 mm). Figure 3a and b correspond to the structure on the transfer element and the target substrate, respectively. A notable feature of this system, illustrated in the SEM images of Figure 3c–e, is that the interconnects remain flat on the surface of the PDMS near the peak of the cone (Figure 3d). The arc shapes increase in curvature from center to edge (Figure 3e). This behavior can be quantitatively related to the local levels of tensile strains in the transfer element in its tensioned, flat membrane geometry. Finite element analysis shows that, as the rim is stretched from 23.6 to 28.9 mm, the strain is small (<1%) around the peak, thereby resulting in flat interconnects. The strains are much larger away from the peak, for example, 10.6% in the meridional direction and 17.5% in the circumferential direction, which leads to buckling of interconnects in these regions (see Supporting Information). Full finite element modeling of the circuit system (without the PI interconnects) integrated with the PDMS transfer element appears in Figure 3f. The results show that the maximum (non-bending) strain in the silicon is ≈0.08%, decreasing with distance toward the center. This behavior indicates that the tensile pre-strain in the periphery of the extended flat PDMS is much larger than that in the central region. The higher strain in the silicon islands at the center is due primarily to bending deformations associated with the small radius of curvature (≈2 mm) in this region. By contrast, the maximum strain in the PDMS is 12.6%, much higher than in the silicon but still far below the fracture strain of PMDS (>150%; see Supporting Information).

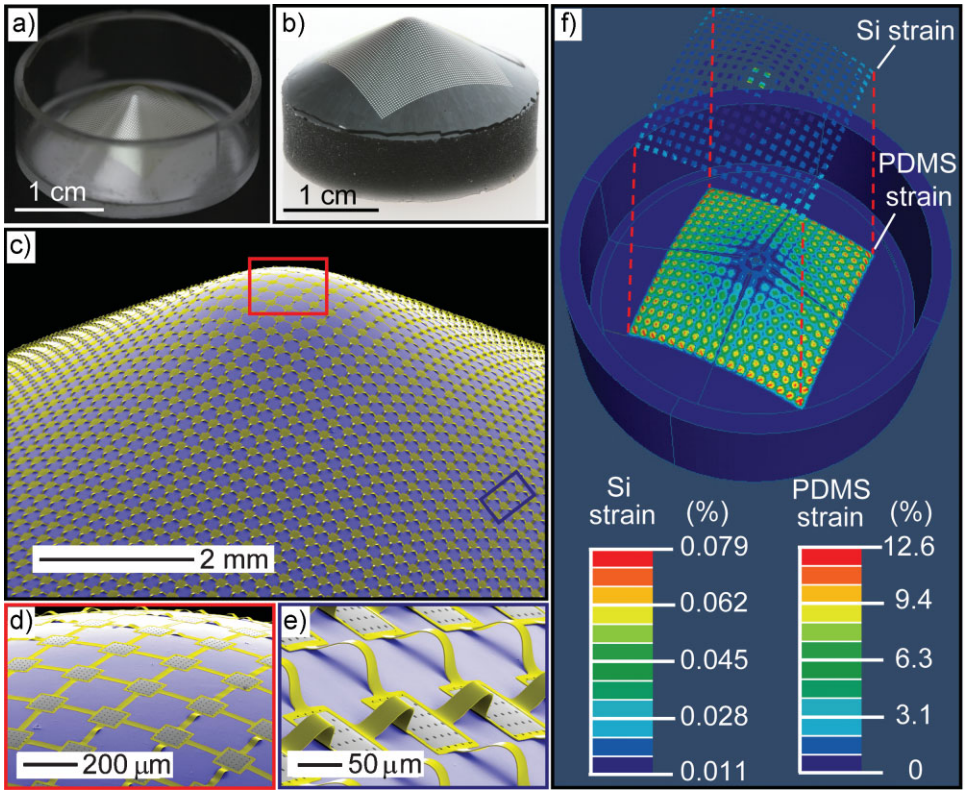

Figure 3. Photographs of a silicon circuit mesh on the surface of a PDMS transfer element with a conical shape before (a) and after (b) transfer to a cone-shaped substrate. c) Angled-view SEM images of the sample shown in (a) and (b). d,e) Magnified angled-view SEM images of the highlighted area of (c). The images were colorized to enhance the contrast of the various regions. The gray, yellow, and blue colors correspond to silicon, PI, and PDMS, respectively. e) Strain distribution obtained by the finite element method in the silicon regions of the circuit and in the underlying PDMS transfer element corresponding to the system shown in (a).

Figure 4a shows the case of a pyramidal substrate (square base with dimensions of ≈16.6 mm × 16.6 mm; height ≈6.5 mm; radius of curvature at the edges ≈1 mm; radius of curvature at the tip ≈1.5 mm) to illustrate additional features of the mechanics. As with the conical surface, the PI interconnects show little or no buckling at the center due to negligible tensile pre-strains in this region. Around the edges of the pyramid, however, different configurations of the interconnects are observed. In particular, the contour shapes include not only single (i.e., global) but multiple (i.e., local) buckling, as highlighted in the SEM images of Figure 4b and c. To gain insight into this behavior, we prepared a 1D array of silicon islands and PI interconnects, transferred them to a thin piece of PDMS under uniaxial tension and then monitored the configurations during release of the tension. The interconnects show multiple buckling with small heights at moderate strains up to ≈8.5%, transforming to a global bucking mode as the small multiple waves merge together at higher strain (see Supporting Information). Mechanical modeling shows that these different behaviors are related to the degree of compressive stress and the adhesion energy between the PI and the PDMS. For stretching of the transfer element from a diameter of 23.6 to 29.8 mm, finite element analysis indicates large strains, 12% ≈ 16%, in the circumferential direction away from the top and four edges of the pyramid. This large strain leads to global buckling observed in Figure 4b. For the same region, the meridional strain is only 2% ≈ 6%. This relatively small strain leads to the type of local bucking observed in Figure 4b. Around the edges of the pyramid, the meridional strain is 6% ≈ 8%, corresponding to local buckling in experiments, while the circumferential strain ranges from 5% to 10%, which results in a mix of local and global buckling. Near the top, both strains are small (<6%) or even compressive, leading to no buckling or some local buckling. These results are consistent with a transition from local and global buckling when the strain reaches about 8%, consistent with experiments on the 1D array (see Supporting Information).

The local buckling results from adhesion between the PDMS membrane and the PI interconnects with a strength that can be characterized by the work of adhesion γ (energy per unit area of the interface). Without any adhesion, the interconnect (length, L; thickness, h) will buckle once the (compressive) strain, $|\varepsilon|$, exceeds the Euler buckling strain[9]

$$\varepsilon_c = \frac{\pi^2 h^2}{3L^2} \tag{1}$$

With adhesion, buckling becomes more difficult since decohesion of interface between the PDMS membrane and the PI interconnect increases the total potential energy, which consists of the membrane and bending energies in the PI and the adhesion energy. As compared to global buckling mode, local buckling decreases the adhesion energy but increases the bending energy. For weak adhesion $\gamma \leq 8Eh\varepsilon_c^2$ (E is the Young's modulus of PI), local buckling never occurs and the (compressive) strain separating global and no buckling is given by (see Supporting Information)

$$For \quad \gamma \leq 8Eh\varepsilon_c^2 \begin{cases} no\ buckling\ if & |\varepsilon| < \varepsilon_c + \sqrt{\frac{2\gamma}{Eh}} \\ global\ buckling\ if & |\varepsilon| \geq \varepsilon_c + \sqrt{\frac{2\gamma}{Eh}} \end{cases} \tag{2}$$

NANO MICRO small

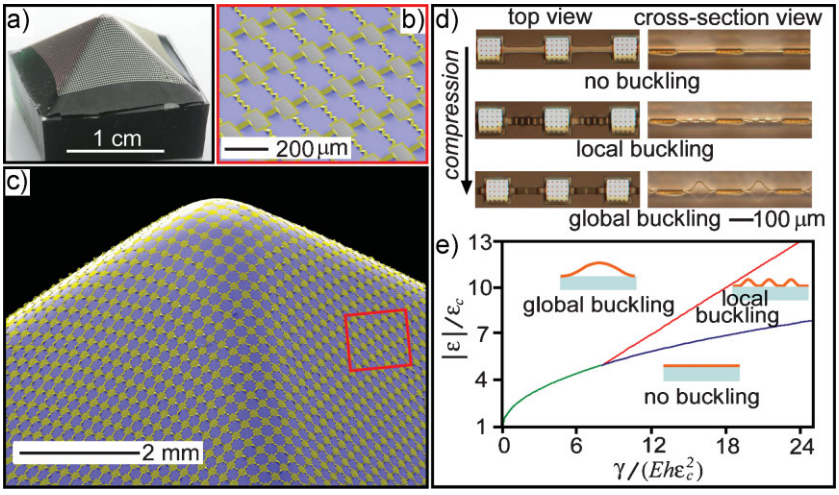

Figure 4. a) Photograph of a silicon circuit mesh wrapped onto a pyramidal substrate. b,c) Colorized angled-view SEM images of the sample shown in (a). b) Magnified view of the area indicated by the box in the right middle region of the image in (c). The gray, yellow, and blue colors correspond to silicon, PI, and PDMS, respectively. d) Top and cross-sectional views of a linear array of interconnected silicon islands on a PDMS substrate subjected, from top to bottom, to low, medium, and high levels of compressive strains. e) The normalized (compressive) strain versus work of adhesion to distinguish different buckling modes.

For relatively strong adhesion, $\gamma > 8Eh\varepsilon_c^2$, the different buckling modes are controlled by

$$For\ \ \gamma > 8Eh\varepsilon_c^2 \begin{cases} no\ buckling & if \quad |\varepsilon| < 5\left(\frac{\gamma\sqrt{\varepsilon_c}}{8Eh}\right)^{2/5} \\ local\ buckling & if\ 5\left(\frac{\gamma\sqrt{\varepsilon_c}}{8Eh}\right)^{2/5} \le |\varepsilon| \le \varepsilon_c + \frac{\gamma}{2Eh\varepsilon_c} \\ global\ buckling & if\ \varepsilon_c + \frac{\gamma}{2Eh\varepsilon_c} < |\varepsilon| \end{cases} \quad (3)$$

The above relations distinguishing different buckling modes are shown in Figure 4e for the normalized strain versus work of adhesion. For the work of adhesion $\gamma = 0.16\,J\,m^{-2}$, which has the correct order of magnitude for PDMS,[10–12] Equation (3) gives the critical strain for local buckling of PI interconnects ($E = 2.5$ GPa; $h = 1.4$ μm; $L = 150$ μm) as 0.78%, which is 27 times the Euler buckling strain ($\varepsilon_c = 0.029\%$). Equation (3) gives the critical strain distinguishing local and global buckling as 8.0%, which agrees reasonably well with 8.5% reported in experiments shown in Figure 4d. These two strains, 0.78% and 8.0%, are also consistent with the ranges of strains for no, local, and global buckling modes observed in golf ball, cone, and pyramid shaped circuit systems (see Supporting Information).

Although the examples described previously involve surfaces with positive curvature, those with negative curvature are also possible. As an example, we created transfer elements in the geometry of paraboloids and wrapped silicon circuit mesh structures onto both the convex (Figure 5a to c) and concave (Figure 5d to e) surfaces (diameter of top circle ≈14.5 mm; height ≈6.9 mm; function for curvature: $y = 0.132\,x^2$) (see Supporting Information). More complex, irregular shapes are also possible. Figure 6a and b demonstrate an example of a target substrate that consists of an anatomically correct, scale model of a heart. As in previous cases, here the interconnects adopt a variety of configurations in different areas, that is, no buckling and multiple waves in the slightly strained area (a red rectangular region of Figure 6c and d) and multiple waves and one pop-up structure in the more highly strained area (a blue rectangular region of Figure 6c and e). The underlying mechanics naturally determine the spatial distributions of these various buckled configurations.

An important aspect of these results is that the mechanics depend only weakly on the presence or absence of active devices, metal electrodes, and other related structures on the islands and interconnecting bridges. To show explicitly the possibility of achieving electrically functional systems, we constructed test structures consisting of circuit meshes with two metal lines encapsulated in PI and contacted to doped silicon islands through vias. The sandwich PI layout places the metal layer near the geometric center of the structure, approximately at the neutral mechanical plane, thereby preventing significant bend induced strains in the metals.[13] Silicon heavily n-doped with phosphorous (P509,

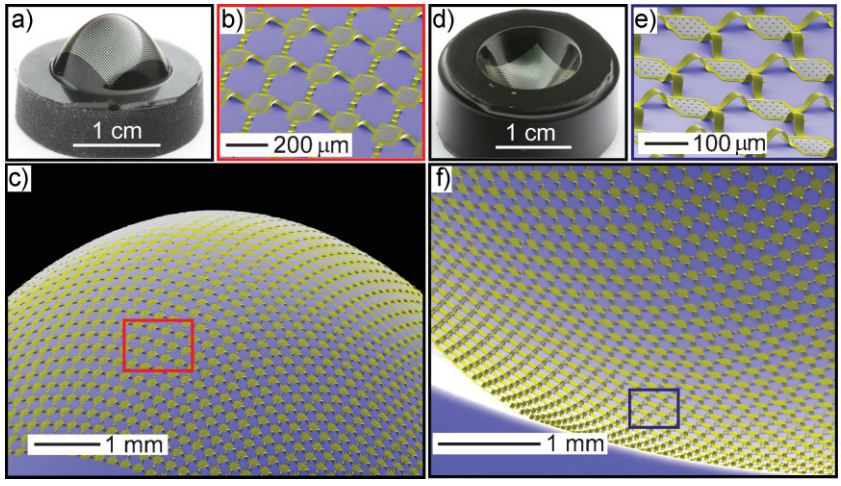

Figure 5. a) Photograph of a silicon circuit mesh on a convex paraboloid substrate. b,c) Colorized angled-view SEM images of the sample shown in (a). b) Magnified view of the area indicated by the box in the center region of (c). d) Photograph of a silicon circuit mesh on a concave paraboloid substrate. e,f) Colorized angled-view SEM images of the sample shown in (d). e) Magnified view of the area indicated by the box in the lower center region of (f). The gray, yellow, and blue colors in the images (b), (c), (e), and (f) correspond to silicon, PI, and PDMS, respectively.

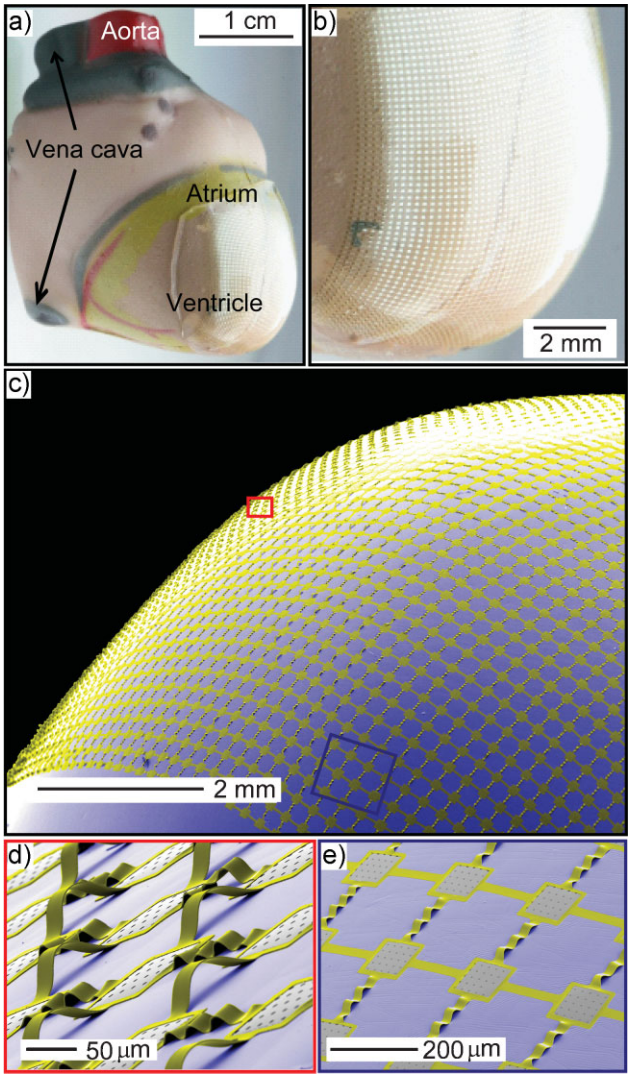

Figure 6. a,b) Photographs of a silicon circuit mesh on a PDMS transfer element on the surface of a plastic model of a human heart. b) Magnified image of (a). c,e) Colorized angled-view SEM images of the sample shown in (a). d,e) Magnified views of the areas indicated by the corresponding boxes in (c). The gray, yellow, and blue colors correspond to silicon, PI, and PDMS, respectively.

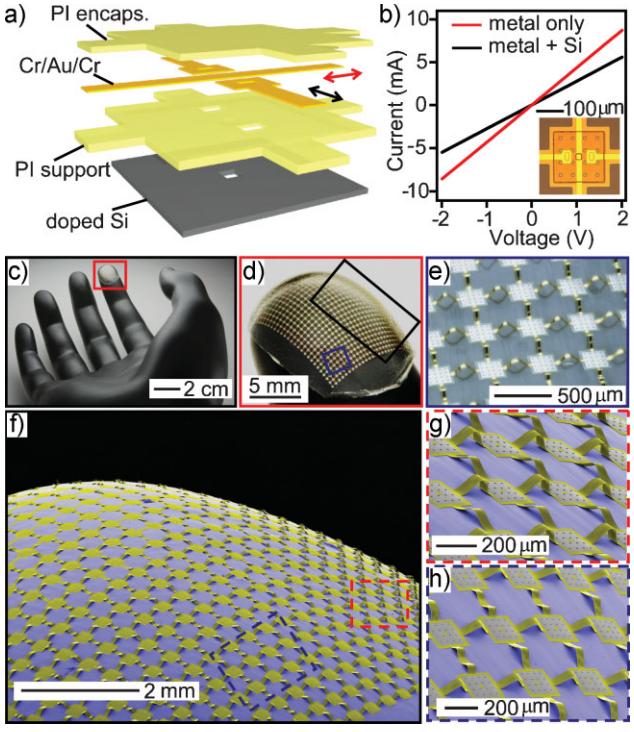

Figure 7. a) Schematic illustration of the layout of the silicon, metal, and polymer layers in a unit cell of a silicon circuit mesh test structure. b) Current–voltage characteristics measured by contacting the continuous metal line (red arrow in (a)) and the discontinuous metal line (black arrow in (a)) at the periphery of the array. The inset shows a top view optical microscopy image of a representative individual island. c,d) Photographs of the circuit mesh transferred onto the tip of a finger on a plastic substrate with the shape of a human hand. d) Magnified view of the region indicated by the box in (c). e) Magnified image of the region indicated by the blue box in (d) collected using a scanning focal technique. f,h) Colorized angled-view SEM images of the sample shown in (c). g,h) Magnified views of areas indicated by the dashed boxes in (f). The gray, yellow, and blue colors correspond to silicon, PI, and PDMS, respectively.

Filmtronics) allows ohmic contact between the metal and the silicon to facilitate electric testing. The mesh in this case consists of a 28×28 array of silicon islands with ends configured for probing. The total number of vias is 1404 (each island has two vias) and the total number of metal lines is 702. The lines are continuous in one direction along the array and discontinuous in the other (see Supporting Information). We wrapped this system onto the fingertip of a life-sized, plastic mannequin hand. Figure 7b shows representative current–voltage curves associated with probing these two directions at the ends of the mesh (Figure 7c to h). The overall yield of electrical connections along the continuous metal lines (the red arrow in Figure 7a) was 99.9% (701 out of 702) and that along the discontinuous (the black arrow in Figure 7a) metal lines and vias was 100% (1404 out of 1404). In most cases presented here, the strain in the device islands is designed to be lower than levels expected to yield significant changes in electrical properties. These results provide clear evidence of the scalability of these approaches to active electronics that could be designed for various applications (e.g., electrotactile stimulation for the case of Figure 7).

3. Conclusions

The work presented here provides strategies for achieving electronics based on high-quality, single-crystalline inorganic semiconductors in geometrical layouts that are impossible using wafer-based technologies. The use of purely elastic mechanics together with hybrid plastic/inorganic circuit meshes enables predictive analysis and high strain deformations, respectively. These aspects represent important distinguishing features compared to related work.[1,2] Experimental and theoretical studies of the underlying micromechanics reveal the capabilities and associated engineering design rules. Future work will focus on refinements that improve the areal coverage of the device islands and enable reduced radii of curvature.

NANO MICRO small

The versatility of these procedures and their compatibility with established semiconductors suggest that they might be useful for applications of electronics or optoelectronics in biomedicine and other areas of application that cannot be addressed using existing technologies.

4. Experimental Section

Formation of a solid, elastomeric replica involves first casting and thermally curing a bulk quantity of liquid prepolymer to an elastomer (PDMS; Dow Corning) against the target substrate. Casting and curing a thin layer of PDMS in the narrow gap between the target substrate (or a derivative surface formed from this substrate) and the replica, while held in an aligned configuration by a specialized mechanical jig, forms a thin (down to ≈100 μm for the experiments described here) membrane with a comparatively thick (≈5 mm) integrated rim around the perimeter. We refer to this structure as an elastomeric transfer element (see Supporting Information).

Si membrane circuits were fabricated with conventional planar processing methods using a SOI wafer (Soitec; thickness of top Si: 700 nm; thickness of SiO_2: 400 nm) to form an array of silicon islands interconnected by narrow strips of PI as interconnects. Removing the buried oxide of the SOI wafer with HF leaves the top circuit layer raised slightly (≈400 nm) above the underlying silicon wafer and supported by PI post structures that exist between the silicon islands (see Supporting Information).

To check the electrical connection between Si islands, the top-silicon of a SOI wafer was heavily doped by spin-on-dopant (P509, Filmtronics). The next steps for isolating the Si islands were the same as above. After subsequent spin-coating (4000 rpm; 60 s) and patterning a PI (Sigma-Aldrich) layer on the silicon islands, metal layers (Cr/Au/Cr) were deposited by sputter coater. Finally, another PI layer was coated on the metal layer with the same procedure to reduce the strain of metal layer when they are compressed. A probe station and parameter-analyzing instrument (Agilent, 4155c) were used in the electrical measurements (see Supporting Information).

Acknowledgements

We thank T. Banks for help in processing by use of facilities at the Frederick Seitz Materials Research Laboratory. The mechanics and materials components of the work were supported by the National Science Foundation under grant ECCS-0824129 and a MURI award. J.S.H. and G.S. acknowledge the Korea Science and Engineering Foundation (KOSEF) through the National Research Lab Program funded by the Ministry of Science and Technology (No. ROA-2007-000-20102-0)

[1] P. J. Hung, K.-H. Jeong, G. L. Liu, L. P. Lee, *Appl. Phys. Lett.* **2004**, *85*, 6051.
[2] R. Dinyari, S.-B. Rim, K. Huang, P. B. Catrysse, P. Peumans, *Appl. Phys. Lett.* **2008**, *92*, 091114/1.
[3] X. Xu, M. Davanco, X. Qi, S. R. Forrest, *Org. Electron.* **2008**, *9*, 1122.
[4] P. I. Hsu, R. Bhattacharya, H. Gleskova, Z. Xi, Z. Suo, S. Wagner, J. C. Sturm, *Appl. Phys. Lett.* **2002**, *81*, 1723.
[5] H.-C. Jin, M. K. Erhardt, R. G. Nuzzo, J. R. Abelson, *J. Vac. Sci. Technol. B.* **2004**, *22*, 2548.
[6] H. C. Ko, M. P. Stoykovich, J. Song, V. Malyarchuk, W. M. Choi, C.-J. Yu, J. B. Geddes, J. Xiao, S. Wang, Y. Y. Huang, J. A. Rogers, *Nature* **2008**, *454*, 748.
[7] T. Someya, Y. Kato, T. Sekitani, S. Iba, Y. Noguchi, Y. Murase, H. Kawaguchi, T. Sakurai, *Proc. Natl. Acad. Sci. U. S. A.* **2005**, *102*, 12321.
[8] S. M. Miller, S. M. Troian, S. J. Wagner, *J. Vac. Sci. Technol. B* **2002**, *20*, 2320.
[9] S. P. Timoshenko, J. M. Gere, *Theory Of Elastic Stability*, McGraw-Hill Book Company Press, New York **1961**.
[10] B. Z. Newby, M. K. Chaudhury, H. R. Brown, *Science* **1995**, *269*, 1407.
[11] Y. Y. Huang, W. X. Zhou, K. J. Hsia, E. Menard, J. U. Park, J. A. Rogers, A. G. A. Alleyne, *Langmuir* **2005**, *21*, 8058.
[12] M. K. Chaudhury, G. M. Whitesides, *Langmuir* **1991**, *7*, 1013.
[13] D.-H. Kim, J.-H. Ahn, W.-M. Choi, H.-S. Kim, T.-H. Kim, J. Song, Y. Y. Huang, L. Zhuangjian, L. Chun, J. A. Rogers, *Science* **2008**, *320*, 507.

Received: June 1, 2009
Revised: August 18, 2009
Published online: October 28, 2009

